High-accuracy robotic metrology for precise industrial manipulation tasks

Mohammed A. Isa*, Mojtaba A. Khanesar, Richard Leach, David Branson, Samanta Piano
Manufacturing Metrology Team, Faculty of Engineering, University of Nottingham, Nottingham, UK

ABSTRACT

The majority of industrial production processes can be divided into a series of object manipulation and handling tasks that can be adapted for robots. Through significant advances in compliant grasping, sensing and actuation technologies, robots are now capable of carrying out human-like flexible and dexterous object manipulation tasks. During operation, robots are required to position objects within tolerances specified for every operation in an industrial process. The ability of a robot to meet these tolerances is the critical deciding factor that determines where the robot can be integrated and how proficient the robot can carry out high-precision tasks. Therefore, improving the positioning accuracy of robots can lead to new avenues for their integration into production industries. Given that tolerances in manufacturing processes are in the order of tens of micrometres or less, robots should guarantee high positioning accuracy when manipulating objects. The direct method of ensuring high accuracy is by introducing an additional measurement system(s) that can improve the inherent joint-angle-based robot position determination. In this paper, we present a high-accuracy robotic pose measurement (HARPM) system based on coordinate measurements from a multi-camera vision system. We also discuss the integration of measurements obtained by absolute distance interferometry and how the interferometric measurements can complement the vision system measurements. The performance of the HARPM system is evaluated using a laser interferometer to investigate robotic positions along a trajectory. The performance results show that the HARPM system can improve the positioning accuracy of robots from hundreds to a few tens of micrometres.

Keywords: Metrology, robotics, accuracy, control, machine vision, interferometry, pose measurement

1. INTRODUCTION

The widespread utilisation of robots in production industries is primarily fuelled by the enhanced economic feasibility they offer in efficiently executing routine tasks[1]. Robots have become indispensable in automating various repetitive operations, resulting in increased productivity and cost-efficiency for businesses[2]. These tasks often involve robot end-effector manipulation operations, where manipulation of the robot end-effector to accurately attain desired positions and configurations is paramount. To proficiently execute multiple manipulation tasks, it is important for robot positioning to not only be repeatable but also accurate[3–5]. However, achieving high-accuracy robotic positioning remains a challenge, which needs to be addressed to expand the industrial use of robots.

Robots play a crucial role in the manufacturing industries for the execution of tasks such as welding, deburring, polishing, grinding, drilling, and inspecting, among others[6]. The economic viability of these industries increasingly relies on the successful deployment of robots for these tasks. To enhance the potential of robots, it is essential to improve their positioning accuracy to broaden their adoption in more demanding applications. The common method of improving robot positioning accuracy is primarily focused on reducing kinematic errors, which often overlook non-kinematic errors, thereby limiting the achievable absolute positioning accuracy[7,8]. To address this limitation, additional measurement sensors, alongside the inherent robot joint-angle-based sensors, have been suggested[9]. Multi-camera systems operating at distances of less than one metre have been demonstrated to enhance robotic positioning; however, even with such systems, positioning errors can still reach magnitudes of hundreds of micrometres or even millimetres[9–11].

To address challenges in robot accuracy, we introduce a high-accuracy robotic pose measurement (HARPM) system that uses a pre-calibrated spatially encoded artefact for robot coordinate measurement. Using the encoded artefact, the HARPM system derives coordinate measurements from the algorithms and methods introduced in our previous work[12,13]. The method for coordinate measurement relies on improved detection, localisation and error reduction strategies applied to multi-view images of the artefact. The comprehensive detection and modelling scheme outlined the work[12] is shown to improve existing methodologies and reduce measurement errors. From accurate photometric positions of target features on the artefact, three dimensional (3D) reconstruction of the features is obtained through triangulation.

In this paper, we extend the application of artefact-based coordinate metrology to include robotic pose measurement and analysis of six degrees of freedom errors. From the coordinate positions of multiple target features on the artefact, orientation information can be derived and tracked. Through increased accuracy, the proposed HARPM improves the measurement of robotic absolute position and orientation, opening up new possibilities for robotic operations with increased accuracy, efficiency and reliability in manufacturing processes and other critical applications.

The following sections provide the methods employed for the proposed HARPM system, where robot positional and angular errors are determined. Investigations of the pose measurement results obtained from verification experiments are described in the results section. By analysing the methodology and results, we aim to demonstrate the effectiveness of the HARPM method in enhancing robotic absolute position, thus paving the way for the broader adoption of robots in manufacturing processes and other applications.

2. METHODS

To accurately measure the pose of a robot, a multi-view measurement approach is employed, which involves capturing images from multiple viewpoints of sphere targets attached to a robot's end-effector. The proposed HARPM solution builds on the vision-based detection and 3D coordinate metrology techniques introduced in our previous work[12]. The vision-based approach uses an artefact with pre-calibrated dimensions and an improved detection algorithm[12], enabling accurate localisation and identification of the artefact sphere features on the robot end-effector.

The uncertainty of measurements obtainable by vision-based methods is usually higher than the uncertainties achievable by interferometric methods. A frequency scanning interferometry (FSI) based technique, shown in Figure 1d), is proposed for robotic measurements alongside the vision system[13]. The concept involves the use of FSI for measurement of the more accuracy-demanding part of the robot trajectory. However, the integration of a FSI system has some drawbacks, such as limited signal intensity, the need for high-bandwidth hardware integration and concerns regarding eye safety[14].

2.1 Vision-based pose measurement

For the spherical artefact targets shown in Figure 1b), using their 3D coordinate positions obtained by the vision-based evaluation[12], we can track six degrees of freedom changes in the robot end-effector. The pre-calibration dataset[15] for the artefact plays a crucial role in this process, providing essential information, such as the sphere-to-sphere distances and diameters. The calibrated dimensions of the eleven sphere targets ($i = 1,2, \dots 11$) fully define the target 3D coordinate positions $\boldsymbol{x}_i^{A_j}$ in the artefact coordinate system at the robot's j^{th} position. As shown in Figure 1a), the artefact coordinate system A_jCS, which is arbitrarily affixed to the centroid of the eleven targets, moves together with the artefact at the twenty positions ($j = 1,2, \dots 20$) along the path of the robot trajectory.

The vision system shown in Figure 1c) consists of three camera views A, B, and C where the stationary vision coordinate system is attached to viewpoint A. The vision system described elsewhere[12] uses images from AB, BC and BC binocular view pairs to triangulate 3D coordinates. The robot path begins from the path number $j = 1$ where the artefact coordinate system starts at the frame A_1CS and moves to an intermediate frame A_jCS. Similar to the vision coordinate system, the

robot coordinate system, from which the joint-sensor-based position measurement of the robot is referenced, is also stationary.

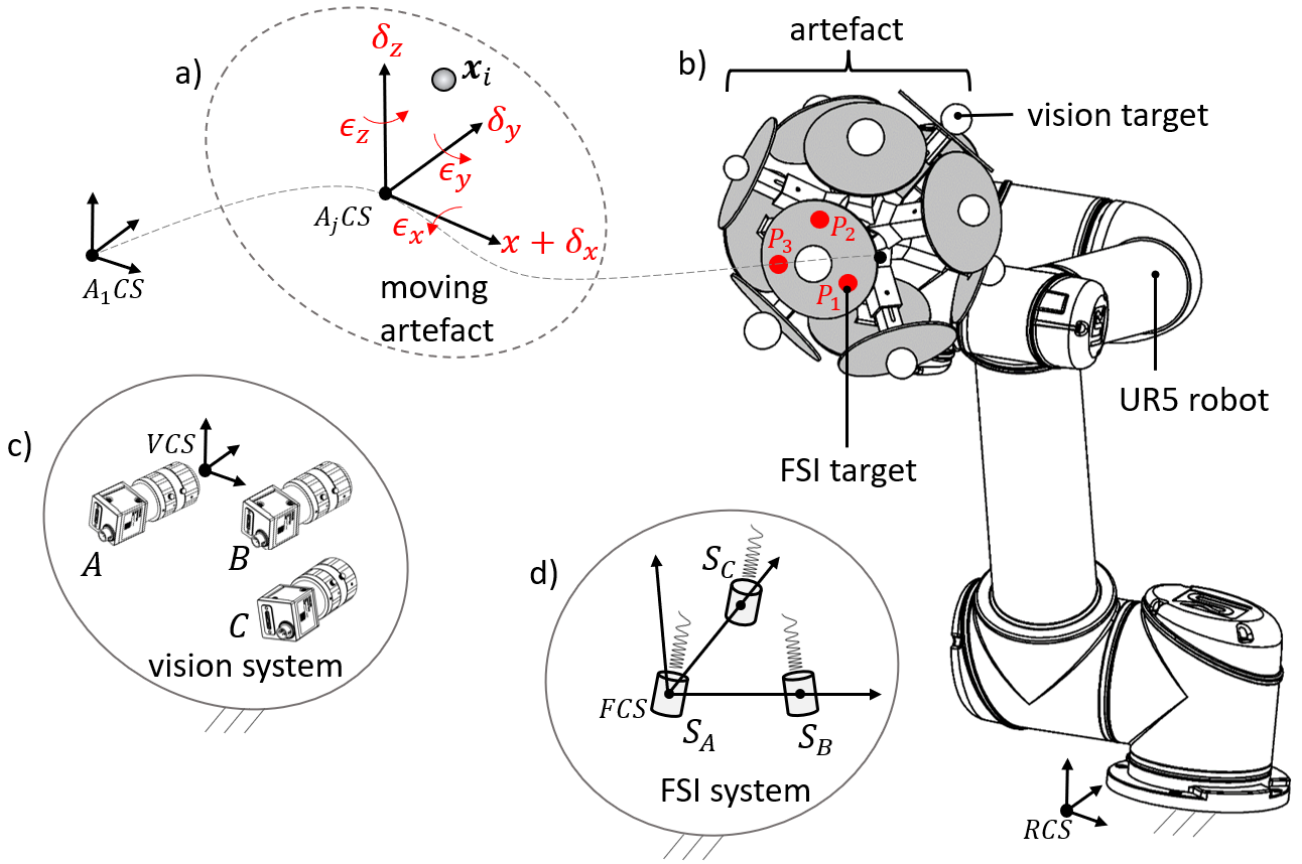

Figure 1. Diagram showing the coordinate system in a) of measurement artefact attached to a robot end-effector in b) where robotic measurements are carried out using the vision system in c) and the FSI system in d).

We assign $\boldsymbol{x}_{i,j}^{V}$ as the 3D coordinate positions of the target i measured by the vision system at the j^{th} robot position along the path shown in Figure 1. At the j^{th} robotic position, the robotic pose is defined by six unknown parameters consisting of three coordinates of position and three angular orientations of the artefact coordinate system. When the robotic pose is evaluated with respect to the vision coordinate system, we can relate target positions $\boldsymbol{x}_{i,j}^{V}$ and $\boldsymbol{x}_{i}^{A_j}$ through

$$\begin{bmatrix} \boldsymbol{x}_{i}^{A_j} \\ 1 \end{bmatrix} = \boldsymbol{T}_{V}^{A_j} \cdot \begin{bmatrix} \boldsymbol{x}_{i,j}^{V} \\ 1 \end{bmatrix}, \tag{1}$$

where $T_{V}^{A_j}$ is the transformation matrix of the vision coordinate system with respect to the artefact coordinate system. The information about the six pose parameters is included in this transformation matrix. Since a minimum of three targets need to be detected in order to evaluate $T_{V}^{A_j}$, the artefact is designed to allow visibility of three or more targets from any orientation[12]. Figure 2a) and b) show the detected sphere targets at the measured coordinate positions in Figure 2d). The spheres are identified using the pre-calibrated artefact dataset. For identification purposes, the adjacency of the sphere targets is expressed in graphs, where the detected spheres are subgraphs of the complete artefact graph, as shown in Figure 2e) and 2f).

From Equation (1), where the transformation matrix $T_{V}^{A_j}$ is unknown, the problem of determining the rigid transform given paired 3D points is encountered. The transformation matrix can be calculated by singular value decomposition (SVD)

when three or more targets are detected[16]. First, the points $\boldsymbol{x}_i^{A_j}$ and $\boldsymbol{x}_{i,j}^{V}$ are translated to their respective centroids and the rotation matrix of $T_V^{A_j}$ is evaluated by SVD. Then, the translation in $T_V^{A_j}$ necessary to satisfy Equation (1) is evaluated using the evaluated rotation matrix.

While determining the pose or transformation of the end-effector with respect to the vision system is valuable, it may not directly provide actionable insights for industrial processes. In practical applications, the goal is often to achieve a specific robotic path or trajectory. Therefore, it becomes critical to evaluate how the actual robotic path aligns with the desired path.

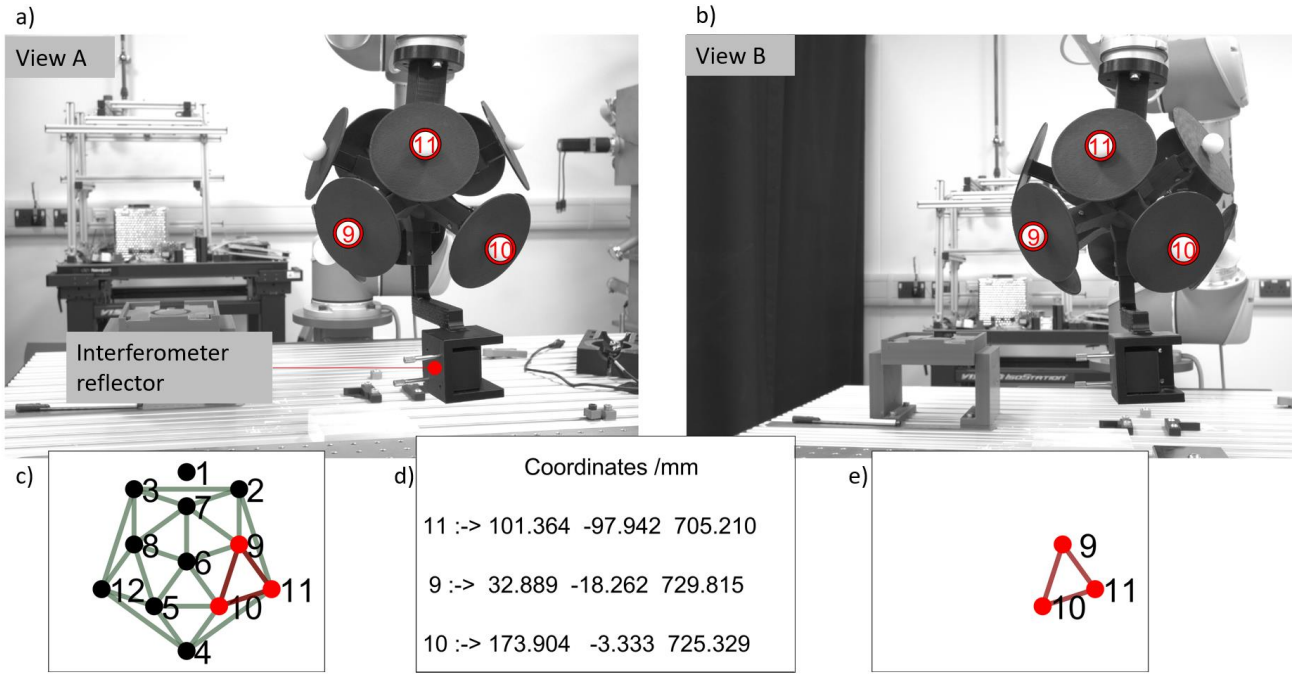

Figure 2. Detected and measured sphere coordinates in d), identified as spheres 9, 10 and 11, are shown from views A in a) and B in b). The subgraph of the identified spheres in e) is overlaid on the overall graph of the pre-calibrated artefact in c). Reflector of a laser interferometer is attached to the target to measure displacements.

2.2 Evaluation of pose measurement error

By comparing the measured poses along a robot trajectory with the desired poses, we can assess the accuracy and performance of the robot in executing the desired path. This evaluation allows for the identification of any discrepancies or deviations from the intended trajectory, from which adjustments can be made accordingly. Pose measurement errors are investigated using a linear robotic path where errors in position and orientation are examined. In this section, the two experiments for robotic displacement and pose measurement are discussed.

In the first experiment, the displacements of a Universal Robots UR5 robotic arm are investigated by evaluating errors in the vision-based HARPM system and the robot in-built (joint-angle-based) measurements. The experiment involves measuring twenty steps of 15 mm robot displacements which is repeated five times. Here, a laser interferometer is employed to measure reference displacements. The laser interferometer used in the experiment is the Renishaw XL-80 model to measure displacements in the measurement travel range of 300 mm. At this specific measurement range, the expanded uncertainty provided by the manufacturer corresponds to ± 0.3 µm (k=2), at the environmental conditions of

0°C, 1150 mbar and 50% relative humidity. For the laser interferometer displacement s_j^{LI} at the j^{th} robot position ($j > 1$), the displacement error of the vision system is expressed as

$$e_v = \left\| \boldsymbol{x}_{i,j}^V - \boldsymbol{x}_{i,j-1}^V \right\| - s_j^{LI}. \tag{2}$$

Similarly, for the in-built robotic coordinate measurement at the j^{th} position $\boldsymbol{x}_j^R$, the displacement error can be expressed as

$$e_r = \left\| \boldsymbol{x}_j^R - \boldsymbol{x}_{j-1}^R \right\| - s_j^{LI}. \tag{3}$$

The second experiment investigates the errors in the six degrees of freedom of motion associated with the vision system pose measurements of the artefact that is attached to a linear actuator. The experiment involves applying nominal step displacements of 25 mm to the linear actuator within its 300 mm travel range. The x-directional measurements obtained from the vision system are then compared to the reference measurements provided by the laser interferometer to obtain the linear error δ_x. The other linear error components of the measurements are the straightness errors which are the y-directional (δ_y) and z-directional (δ_z) error components. The directions of the errors are shown in Figure 1.

Considering the artefact (and robot end-effector) coordinate system A_1CS that moves to a new coordinate system A_jCS through a linear displacement of $x = s_j^{LI}$ along the x-direction of A_1CS, we can represent the transformation matrix of A_jCS with respect to A_1CS as

$$\boldsymbol{T}_{A_j}^{A_1} = \boldsymbol{T}_V^{A_1} \cdot \boldsymbol{T}_V^{A_j{}^{-1}}, \tag{4}$$

where $\boldsymbol{T}_V^{A_j}$ can be determined using the method described in Section 1.1. The linear direction of motion, contained in $\boldsymbol{T}_{A_j}^{A_1}$ is used to reevaluate $\boldsymbol{T}_{A_j}^{A_1}$ using Equation (4) after the orientation of A_1CS is aligned such that the x-direction of A_1CS coincides with the linear direction of motion of the actuator. The linear error components $[\delta_x \quad \delta_y \quad \delta_z]^\top$ are then evaluated from the elements of $\boldsymbol{T}_{A_j}^{A_1}$ as

$$\begin{bmatrix} \delta_x \\ \delta_y \\ \delta_z \end{bmatrix} = \begin{bmatrix} T_{A_j}^{A_1}(4,1) - s_j^{LI} \\ T_{A_j}^{A_1}(4,2) \\ T_{A_j}^{A_1}(4,3) \end{bmatrix}, \tag{5}$$

where $T_{A_j}^{A_1}(n,m)$ denotes the element at the n^{th} row and the m^{th} column of the transformation matrix $T_{A_j}^{A_1}$. The angular error components $[\epsilon_x \quad \epsilon_y \quad \epsilon_z]^\top$ represent the roll, pitch and yaw degrees of freedom of motion and can be expressed by the Euler angles given by

$$\begin{bmatrix} \epsilon_x \\ \epsilon_y \\ \epsilon_z \end{bmatrix} = \begin{bmatrix} \tan^{-1}\left(\dfrac{T_{A_j}^{A_1}(3,2)}{T_{A_j}^{A_1}(3,3)}\right) \\ \tan^{-1}\left(-\dfrac{T_{A_j}^{A_1}(3,1)}{\sqrt{T_{A_j}^{A_1}(3,2)^2 + T_{A_j}^{A_1}(3,3)^2}}\right) \\ \tan^{-1}\left(\dfrac{T_{A_j}^{A_1}(2,1)}{T_{A_j}^{A_1}(1,1)}\right) \end{bmatrix}. \tag{6}$$

Equations (5) and (6) present the degree-of-freedom errors of the vision system and indicate the performance of the vision system in accurately measuring the pose of the artefact.

3. RESULTS AND DISCUSSION

In this section, we present the analysis of results using the pose error evaluation methods described in Section 2.2. First, we use the displacement errors described in Equations (2) and (3) to examine the distribution of errors, as shown in Figure 3. Specifically, Figure 3a) displays the errors in displacements obtained by the in-built robot coordinates, while Figure 3b) showcases the errors in displacements obtained by the HARPM system coordinates. Upon observation, it becomes evident from the standard deviation that the vision coordinates are more accurate than those obtained by the in-built measurement coordinate systems. This finding highlights the capability of the HARPM vision system to enhance the precision of robotic positions. Additionally, it should be noted that in applications where the robot is subjected to additional forces, the accuracy of the in-built coordinates tends to deteriorate due to added kinematic errors. However, the vision system remains unaffected by such errors.

The displacement results compare the error of the robot's inherent measurement system with that of the vision system for unidirectional displacement measurements, using reference displacements measured by the laser interferometer. This experimental comparison provides evidence that the vision measurement system can outperform the internal robot's measurement system.

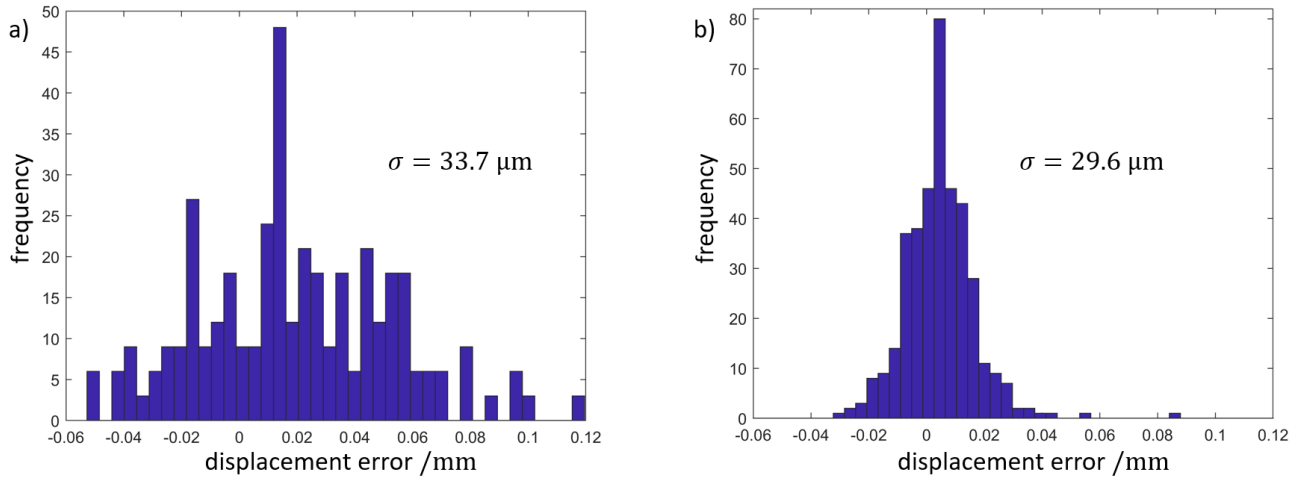

Figure 3. Displacement error distribution of a) in-built robot coordinates and b) measured vision system coordinates for 15 mm displacements using AB, BC and BC binocular vision. The standard deviation of the error distributions are given by the indicated values of σ.

In addition to assessing the unidirectional distance error, a comprehensive evaluation of the six degrees of freedom error is conducted. This evaluation involves measuring the pose of the artefact and comparing it to the nominal trajectory. To achieve this, we utilise an actuator that provides linear motion. The linear actuator has been designed to minimise errors, with straightness errors below 20 µm and angular errors below 1 mrad[17,18]. By employing this linear motion, we can accurately quantify any variations in the measured pose of the artefact across all six degrees of freedom.

The values of the linear and angular pose error measured by the HARPM are shown in Figure 4. Figures 4a), 4b) and 4c) show the linear error components while Figures 4d), 4e) and 4f) show the angular error components for the AB, AC and BC binocular vision systems illustrated in Figure 1c). The results shown in Figure 4 indicate that the BC binocular vision system results in slightly higher error compared to the other parings, probably because the BC vision system has the

shortest baseline. The 3D coordinates triangulated from short baselines have been reported to be less accurate[18]. The AB and AC binocular vision systems have linear distance errors that are mostly less than 100 µm, straightness errors that are below 200 µm and angular errors that largely less than 1.5 mrad. It is noteworthy that the straightness and angular errors contain the kinematic errors of the linear actuator. Besides excluding binocular systems with short baselines, pose errors can be further reduced when a trinocular vision system that integrates the three binocular vision systems is implemented.

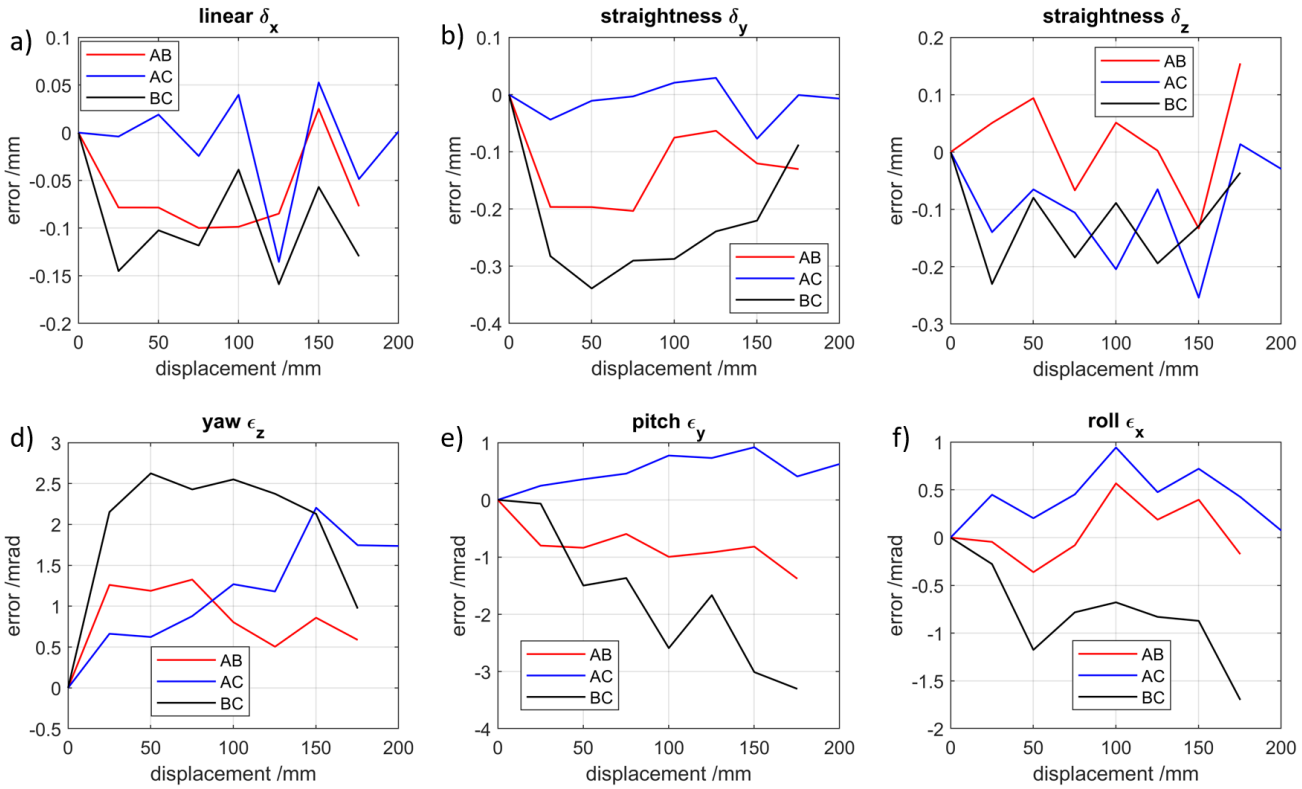

Figure 4. Linear and angular error results of the measured artefact pose along a linear path. For AB, AC and BC binocular vision systems, the errors shown are a) linear distance error, b) straightness error along y-direction, c) straightness error along z-direction, d) yaw angular error, e) pitch angular error and f) roll angular error.

4. CONCLUSION

Acknowledging the demand for the use of robots in high-precision industrial tasks, we present high-accuracy robotic pose measurement to improve industrial manipulation and handling of objects. We verify the performance of the measurement system using an interferometer and a linear actuator. The measurement system can be integrated into industrial robots for use in high-precision tasks where tolerance requirements are not guaranteed without the measurement system. From the performance verification of the system, it is possible to measure pose changes in the scale of 10 µm for linear displacements and 0.1 mrad for rotational displacements. It is also shown that the proposed coordinate measurement system outperforms the robot in-built coordinate system for displacement measurements. Further research and development in this area could lead to significant advancements in robotic metrology and enable the realisation of precise and flexible object manipulation tasks in various industries.

Acknowledgements: This work is funded by the Engineering and Physical Sciences Research Council (EPSRC) under grant number: EP/T023805/1 HARISOM. The authors would like to thank UKRI Research England Development (RED) Fund for assisting this work via the Midlands Centre for Data-Drive Metrology.

REFERENCES

[1] De Vries G.J., Gentile E., Miroudot S. and Wacker K.M. 2020 The rise of robots and the fall of routine jobs *Labour Econ.* **66** 101885 doi:https://doi.org/10.1016/j.labeco.2020.101885

[2] Möller C., Christian H. and Hasmukhbhai N. 2016 Enhanced absolute accuracy of an industrial milling robot using stereo camera system *Procedia Technol.* **26** 389–98 doi:10.1016/j.protcy.2016.08.050

[3] Garnier S. and Subrin K. 2022 A metrological device for robot identification *Robot. Comput. Integr. Manuf.* **73** 102249 doi:https://doi.org/10.1016/j.rcim.2021.102249

[4] Khanesar M.A., Yan M., Isa M., Piano S. and Branson D.T. 2023 Precision Denavit–Hartenberg Parameter Calibration for Industrial Robots Using a Laser Tracker System and Intelligent Optimization Approaches *Sensors* **23** doi:10.3390/s23125368

[5] Pollák M., Kočiško M., Paulišin D. and Baron P. 2020 Measurement of unidirectional pose accuracy and repeatability of the collaborative robot UR5 *Adv. Mech. Eng.* **12** 1687814020972893

[6] Kinnell P., Rymer T., Hodgson J., Justham L. and Jackson M. 2017 Autonomous metrology for robot mounted 3D vision systems *CIRP Ann.* **66** 483–6 doi:https://doi.org/10.1016/j.cirp.2017.04.069

[7] Jiang Y., Yu L., Jia H., Zhao H. and Xia H. 2020 Absolute Positioning Accuracy Improvement in an Industrial Robot *Sensors* **20** 4354 doi:10.3390/s20164354

[8] Khanesar M.A., Yan M., Kendal P., Isa M., Piano S. and Branson D. 2023 Intelligent Static Calibration of Industrial Robots using Artificial Bee Colony Algorithm *2023 IEEE International Conference on Mechatronics (ICM)* 1–6 doi:10.1109/ICM54990.2023.10101918

[9] Liu B., Zhang F. and Qu X. 2015 A Method for Improving the Pose Accuracy of a Robot Manipulator Based on Multi-Sensor Combined Measurement and Data Fusion *Sensors* **15** 7933–52 doi:10.3390/s150407933

[10] Du G. and Zhang P. 2013 Online robot calibration based on vision measurement *Robot. Comput. Integr. Manuf.* **29** 484–92 doi:https://doi.org/10.1016/j.rcim.2013.05.003

[11] He Z., Wu M., Zhao X., Zhang S. and Tan J. 2021 A Generative Feature-to-Image Robotic Vision Framework for 6D Pose Measurement of Metal Parts *IEEE/ASME Trans. Mechatronics* 1–12 doi:10.1109/tmech.2021.3109344

[12] Isa M.A., Leach R., Branson D. and Piano S. 2023 Vision-based detection and coordinate metrology of a spatially encoded multi-sphere artefact [manuscript submitted]

[13] Isa M.A., Khanesar M.A., Leach R., Branson D. and Piano S. 2022 Frequency scanning interferometry for accurate robot position measurement *EUSPEN* (Geneva) 305–8

[14] Sosin M., Mainaud-Durand H., Rude V. and Rutkowski J. 2019 Frequency sweeping interferometry for robust and reliable distance measurements in harsh accelerator environment *Proc.SPIE* **11102** doi:10.1117/12.2529157

[15] Isa M.A. 2023 *Vision and laser-interferometry metrology dataset of a spatially encoded target* (The University of Nottingham) doi:10.17639/NOTT.7284

[16] Arun K.S., Huang T.S. and Blostein S.D. 1987 Least-Squares Fitting of Two 3-D Point Sets *IEEE Trans. Pattern Anal. Mach. Intell.* **PAMI-9** 698–700 doi:10.1109/TPAMI.1987.4767965

[17] Isa M.A., Sims-waterhouse D., Piano S. and Leach R.K. 2019 Kinematic error analysis of stage tracking using stereo vision *Proc. ASPE* 151–7

[18] Isa M.A., Sims-Waterhouse D., Piano S. and Leach R.K. 2020 Volumetric error modelling of a stereo vision system for error correction in photogrammetric three-dimensional coordinate metrology *Precis. Eng.* **64** 188–99 doi:10.1016/j.precisioneng.2020.04.010